Chinese Chemical Letters 35 (2024) 109601

Contents lists available at ScienceDirect

Chinese Chemical Letters

journal homepage: www.elsevier.com/locate/cclet

Rationally engineered IR-783 octanoate as an enzyme-activatable fluorogenic tool for functional imaging of hNotum in living systems

Lilin Song[a,c,1], Mengru Sun[b,1], Yuqing Song[b], Feng Zhang[b], Bei Zhao[b], Hairong Zeng[b], Jinhui Shi[b], Huixin Liu[d], Shanshan Zhao[e], Tian Tian[b,*], Heng Yin[a,c], Guangbo Ge[b,*]

[a] Liaoning Provincial Key Laboratory of Carbohydrates, Dalian Institute of Chemical Physics, Chinese Academy of Sciences, Dalian 116023, China
[b] Shanghai Frontiers Science Center of TCM Chemical Biology, Institute of Interdisciplinary Integrative Medicine Re-search, Shanghai University of Traditional Chinese Medicine, Shanghai 201203, China
[c] University of Chinese Academy of Sciences, Beijing 100049, China
[d] Health Sciences Institute, China Medical University, Shenyang 110122, China
[e] Department of Gynecology, Cancer Hospital of China Medical University, Liaoning Cancer Hospital & Institute, Shenyang 110042, China

ARTICLE INFO

Article history:
Received 24 October 2023
Revised 29 January 2024
Accepted 30 January 2024
Available online 4 February 2024

Keywords:
hNotum
Optical substrate
Computer-aided molecular design
In-situ functional imaging
Cancer diagnosis

ABSTRACT

As a vital negative regulator of Wnt signaling pathway, human Notum (hNotum) plays a crucial regulatory role in the progression of many human diseases. Deciphering the relevance of hNotum to human diseases requires practical and reliable tools for visualizing hNotum activity in living systems. Herein, an enzyme-activatable fluorogenic tool (**IR-783 octanoate**) was rationally engineered for sensing and imaging hNotum activity in living systems by integrating computer-aided molecular design and biochemical assays. **IR-783 octanoate** showed good optical properties, excellent specificity and high binding-affinity towards hNotum ($K_m = 0.98$ μmol/L). **IR-783 octanoate** could be well up-taken into the cancerous cells or tumors that over-expressed organic anion transporting polypeptides (OATPs), and then hydrolyzed by cellular hNotum to release free **IR-783 ketone**, which created brightly fluorescent signals around 646 nm. Further investigations showed that **IR-783 octanoate** achieved a good performance for *in-situ* functional imaging of hNotum in both living cells, cancerous tissues and organs. It was also found that some SW620 cells with multipolar spindles could be stained by **IR-783 octanoate** to emit extremely bright signals, suggesting that this agent could be used as a novel visualizing tool for tracing the cells undergoing abnormal cell mitoses. Collectively, this study devises a highly specific fluorogenic tool for *in-situ* functional imaging of hNotum in living systems, which offers a practical and reliable tool to dynamically track the changes in hNotum activity under various conditions.

Human Notum (hNotum), a secreted extracellular palmitoleoyl protein carboxylesterase, is known for regulating the Wnt signaling pathway by a negative feedback mechanism and is implicated in many physiological processes [1–5]. Under physiological conditions, hNotum removes the palmitoleoyl of mature Wnt proteins and destroys the affinity between Wnt proteins and their receptors (such as Frizzled receptor), thereby down-regulates the Wnt signaling pathway [4,6–8]. As a key regulator of Wnt signaling pathway, hNotum plays crucial roles in the progression of a suite of human diseases, including Alzheimer's disease [9,10], osteoporosis [11–14], intestinal diseases [15,16] and *Apc*-mutant colorectal cancer [5,17]. Recent investigations have revealed that hNotum could also regulate or interact with other tumor-associated signaling pathways including Hedgehog signaling pathway [18], phosphoinositide 3-kinase-Ak strain transforming (PI3K/AKT) signaling pathway [19] and transforming growth factor-beta (TGF-β) signaling pathway [5], which in turn, regulating the tumorigenesis, stemness and progression across various tumor types. Although it has been reported that hNotum is overexpressed in multiple cancers, such as primary hepatocellular carcinoma [20], gastric cancer [19], colorectal cancer [5,17,21–24] and oral squamous cell carcinoma [18], the relevance of hNotum to malignancies and other human diseases have not been fully investigated.

Tracking and visualizing the dynamical changes in hNotum activity in living systems under various conditions will strongly facilitate the scientists to deeply understand the biological roles of hNotum in the progression of a suite of human diseases. To decipher

* Corresponding authors.
E-mail addresses: tiantian@shutcm.edu.cn (T. Tian), geguangbo@shutcm.edu.cn (G. Ge).
[1] These authors contributed equally to this work.

https://doi.org/10.1016/j.cclet.2024.109601
1001-8417/

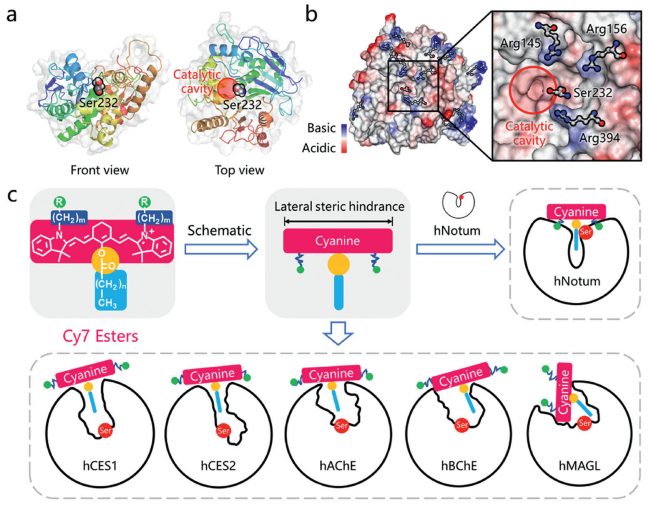

Fig. 1. (a) The location of catalytic Ser232 in hNotum (PDB ID: 6ZYF). (b) The distribution of ionizability and arginine residues on the surface of hNotum (PDB ID: 6ZYF). Three basic arginine residues are surrounding catalytic Ser232. (c) A design concept of "T-shaped" Cy7 esters as new generation optical substrates for highly selective sensing hNotum, the shape of enzyme active cavity was portrayed according to the published crystal structure.

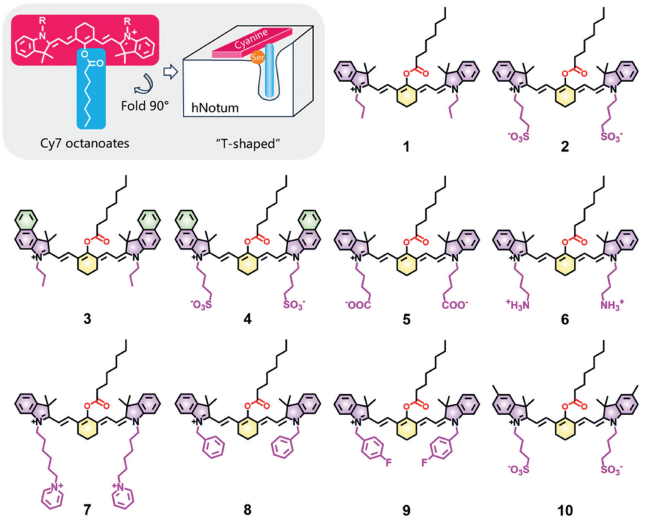

Fig. 2. Structures of the designed cyanine octanoates for searching the most suitable hNotum substrates.

the revelation of hNotum activity to human diseases, the practical and reliable tools for sensing and visualizing hNotum activity in living systems are highly desirable [25]. Currently, trisodium 8-octanoyloxypyrene-1,3,6-trisulfonate (OPTS) is the most commonly used optical substrate for hNotum, but it could not be applied in living systems owing to its poor selectivity [26,27]. More recently, our groups have successfully devised two optical substrates for hNotum, namely octanoyl luciferin (OL) [28] and 3-*O*-methyl-6-*O*-octanoylfluorescein (MOF) [29]. As a bioluminescent substrate, OL cannot be used for functional imaging of hNotum at the subcellular level with high spatial resolution, while the detection wavelength of MOF is less than the first biological transparency window (650–950 nm) [30], which greatly limit their applications in living systems. Thus, the practical hNotum optical substrates with excellent specificity, long detection wavelengths and high spatial resolution are highly desirable.

Previous studies have revealed that hNotum prefers to hydrolyze chemically diverse octanoates, from small molecules (such as *p*-nitrophenol octanoate, octanoyl luciferin) to biomacromolecules (such as octanoylated ghrelin) [7,28,31]. The substrate promiscuities of hydrolases pose a significant challenge in developing highly specific optical tools for hNotum in the presence of various esterases in humans. It is noteworthy that the catalytic center of hNotum, Ser232, is located at the entrance of the catalytic cavity (Fig. 1a), whereas the catalytic serine residues of other human serine hydrolases, such as carboxylesterases (CESs) and cholinesterases (ChEs), are typically found in the deeper parts of the catalytic cavity (Fig. 1c and Fig. S2 in Supporting information). The superficial location of catalytic Ser232 in hNotum allows for less stringent restrictions on the sizes of the alcohol moieties of substrates compared to other esterases, which are usually limited by the shapes of their catalytic cavities. This unique structural feature suggests that it is feasible to design some "T-shaped" esters (Figs. 1c and 2) as highly specific substrates for hNotum, by introducing a significant lateral steric hindrance surrounding the ester group.

Following reviewing the structural features of the commonly used fluorescent dyes with long emission wavelengths and excellent photophysical properties, we found that heptamethine cyanine (Cy7) dyes are ideal skeletons for developing hNotum substrates [32–37]. Firstly, the modifiable chlorines of Cy7 dyes are situated in the middle of heptamethine chains and can be easily modified to form "T-shaped" Cy7 esters [38]. As shown in Fig. 2, when neglecting the *N*-substituent of cyanine esters, the cyanine skeleton with lateral planar conjugated structures looks like a long plank, which is simplified as the horizontal line of the letter T; the fatty acyl group is located at the mesoposition of cyanine sleleton, it looks like the vertical line of letter T. Therefore, the cyanine esters were termed as "T-shaped" molecules. Secondly, the *N*-substituent groups of Cy7 esters can be further improved to enhance their binding affinities towards hNotum by enhancing the interactions with the residues on the surface of hNotum (Figs. 1b and c) [32–34]. Moreover, Cy7 ketones generate brightly fluorescence signals with long-wavelength emission that fall within the first biological transparency window (650–950 nm), making them advantageous for imaging in living systems due to their high signal-to-noise ratios and deep tissue penetration [30,38]. In brief, Cy7 esters are excellent candidates for designing and developing fluorescent substrates for hNotum, due to their ideal structural features and excellent optical properties. To validate this assumption ("T-shaped" Cy7 esters were ideal hNotum substrates), a suite of Cy7 octanoates (Fig. 2) were designed, while computer-aided molecular design (CAMD) technology was used to assess the potentials of these Cy7 esters as hNotum substrates.

To evaluate the potentials of the designed Cy7 esters as hNotum substrates, each ligand was docked into the catalytic cavity of hNotum and then ranked based on the minimum ΔG of all hydrolytic conformations. The hydrolytic conformations should meet the following two requirements. Firstly, the distance between the ester bond and hNotum catalytical Ser232 should be less than 3.3 Å to allow nucleophilic attack by Ser232 [7]. Secondly, the octanoyl groups of the esters should be located in the hydrophobic pocket of hNotum. As shown in Table S2 (Supporting information), ligands 8 and 9 were excluded initially due to the lack of any hydrolytic conformations. Ligands 2 and 4 exhibited remarkably high binding-affinities with hNotum, both esters carried *N*-butylsulfonyl groups. However, ligand 10, which also had two *N*-butylsulfonyl groups, did not show a high affinity towards hNotum, possibly due to the steric hindrance caused by the methyl groups.

To investigate the influence of *N*-butylsulfonyl on the binding modes of ligands 2 and 4, molecular dynamics (MD) simulations and the molecular mechanics/Poisson–Boltzmann surface area (MM/PBSA) analyses were performed [39]. Fig. S3a

(Supporting information) illustrated the unstable binding of ligand 4 to hNotum, which likely cause by the significant steric hindrance of benzoindole moieties. In the case of ligand 2, Arg145, Arg156 and Arg394 made significantly larger contributions compared to other residues (Fig. S3b in Supporting information). As shown in Fig. S3c (Supporting information), three arginine residues could interact with the sulfonic tails *via* Coulomb interactions. Despite the octanoyl group of ligand 4 leaving the hydrophobic pocket during MD simulations, the sulfonic tails of ligand 4 remained tightly bound to these arginine residues, keeping ligand 4 on the surface of hNotum (Figs. S3b and d in Supporting information). Correspondingly, ligands 6 and 7 with alkaline *N*-substituent groups exhibited the worst ΔG values, while ligand 5 with less acidic *N*-butylcarboxyl moieties also had a higher ΔG than ligand 2. These findings reinforce the notion that the interactions between *N*-butylsulfonyl groups and the arginine residues on the surface of hNotum primarily contributes to the tight binding of ligand 2 or 4 with hNotum (Table S2). Notably, parts of the arginine residues located on the surface of hNotum also play key roles on the binding of endogenous glypicans bearing sulfated glycans [7], which inspired us to improve the binding affinity of substrate candidates by introducing sulfonyl groups on Cy7 esters. In this study, it is also found that *N*-butylsulfonyl groups of both ligands 2 and 4 could create strong interactions with the arginines surrounding the catalytic Ser232, suggesting that these *N*-butylsulfonyl groups play a crucial role in improving the binding affinities of these two ligands with hNotum.

To predict the specificities of ligands 2 and 4 towards hNotum, these two esters were then docked with six other abundant serine hydrolases in humans. As shown in Table S3 (Supporting information), both ligands 2 and 4 could not form any hydrolytic conformations in these six human esterases (including human carboxylesterase 1, hCES1; human carboxylesterase 2, hCES2; human acetylcholinesterase, hAChE; human butyrylcholineesterase, hBChE; human monoacylglycerol lipase lipases, hMAGL and human alpha/beta-hydrolase domain-containing 6, hABHD6), showing inherent specificities towards hNotum due to their unique "T-shaped" structure. Encouraged by these findings, two Cy7 esters (**IR-783 octanoate** (ligand 2) and **IR-820 octanoate** (ligand 4)) were successfully synthesized as potential substrates for hNotum, while their structures were fully characterized (Figs. S9–S23 in Supporting information).

It has been reported that the corresponding Cy7 ketones would be released from Cy7 esters after ester bonds breaking [40–51]. Accordingly, the absorption and emission spectra of the hydrolytic product of either **IR-783 octanoate** or **IR-820 octanoate** (namely **IR-783 ketone** and **IR-820 ketone)** were measured. As shown in Figs. S4a–d (Supporting information), the maximum excitation/emission wavelengths of **IR-783 ketone** and **IR-820 ketone** were determined as 564 nm/646 nm and 590 nm/674 nm, respectively. The maximum emission wavelengths of both Cy7 ketones were much longer than two previously reported hNotum optical substrates (OL and MOF) [28] and near the first biological transparency window. Upon addition of hNotum, dramatic increases of fluorescence intensities were observed at the maximum excitation/emission wavelengths of the corresponding ketone products for both **IR-783 octanoate** and **IR-820 octanoate**, confirming that hNotum catalyzed the formation of the corresponding ketone products from Cy7 esters. It was also evident from Figs. S4b, d and e (Supporting information) that compared to **IR-820 octanoate**, **IR-783 octanoate** triggered much greater fluorescence enhancement under same conditions, suggesting that **IR-783 octanoate** was a rapid response optical substrate for hNotum.

Considering that **IR-783 ketone** undergoes a pH-sensitive conversion between enol form and ketone form, it is important to investigate the changes in excitation/emission wavelengths at different pH values [38]. As shown in Fig. S4f (Supporting information), the fluorescent intensity of IR-783 octanoate was very weak at various pH values, suggesting that this ester was chemical stably over a wide range of pH. By contrast, **IR-783 ketone** emitted brightly fluorescence signals when pH over 7.0, suggesting that this agent could work well under physiological conditions. These findings suggested that **IR-783 octanoate** was a rapid response substrate for hNotum and this agent could work well under physiological conditions.

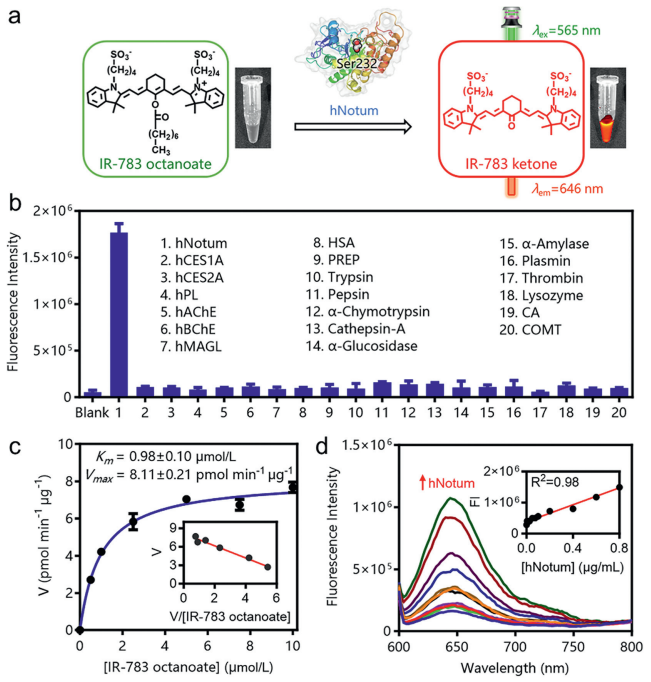

Fig. 3. (a) The mechanism of IR-783 octanoate as hNotum optical substrates. (b) Specificity of IR-783 octanoate to hNotum, $P < 0.0001$. (c) The Michael-Menten curve and the Eadie-Hoftsee plot of Notum-mediated IR-783 octanoate hydrolysis. (d) Liner response between fluorescence signals of IR-783 octanoate and the hNotum concentrations. Error bars represent mean ± standard deviation (SD).

Upon addition of hNotum, **IR-783 octanoate** could be readily hydrolyzed to release **IR-783 ketone**, which created brightly signals around 646 nm (Fig. 3a). The specificity of **IR-783 octanoate** towards hNotum was further examined using a suite of human hydrolases. As shown in Fig. 3b, only hNotum could trigger significant fluorescence enhancement under physiological conditions. In sharp contrast, multiple human esterases and other human proteins with hydrolytic activity hardly trigger fluorescence enhancement around 646 nm. These results clearly demonstrated that **IR-783 octanoate** was a highly specific fluorogenic substrate for hNotum, suggesting that the "T-shaped" molecule design strategy was well-suited for developing the highly specific fluorogenic substrates for this target serine hydrolase. **IR-783 octanoate** hydrolysis in hNotum presented canonical Michaelis-Menten kinetics, with the Michaelis-Menten constant (K_m) of 0.98 ± 0.10 μmol/L and the maximal reaction velocity (V_{max}) value of 8.11 ± 0.21 μmol min^{-1} μg $protein^{-1}$ (Fig. 3c). These findings suggested that **IR-783 octanoate** was a specific substrate for hNotum with high binding-affinity.

As shown in Fig. 3d, the fluorescent signals around 646 nm exhibited a strong correlation with increasing concentrations of hNotum, enabling the determination of hNotum activity in different samples with a robust linear response. These finding clearly demonstrated that **IR-783 octanoate** was an ideal enzyme-activable optical substrate for hNotum, showing high binding-affinity and excellent enzyme specificity. These favorable charac-

teristics motivated us to utilize it for *in-situ* functional imaging of hNotum in living systems.

Next, three different types of tumor cells (including Caco-2, OE19 and SW620 cells) were used for imaging the cellular hNotum at the subcellular level, by utilizing **IR-783 octanoate** as a fluorogenic tool. As shown in Fig. 4a, relatively weak red fluorescence signals were observed in Caco-2 cells, while the red signals predominantly localized at the edges of cell clusters. In sharp contrast, upon addition of **IR-783 octanoate**, the red fluorescence signals in OE19 and SW620 cells were observed in both cell membrane and cytoplasm. Among three tested cells, the fluorescent intensities inside from SW620 cells was much higher than that in OE19 and Caco-2 cells. It is well-known that Caco-2 cells (derived from primary colorectal adenocarcinoma) display significant epithelial cell differentiation characteristics, while SW620 cells (derived from lymphatic node metastasis of human colorectal adenocarcinoma) exhibit a higher metastatic potential compared to Caco-2 cells [52]. The different hNotum activity in these cell lines determined by **IR-783 octanoate** also implied that hNotum was closely associated with the progression of colorectal cancers [5,17,21–24]. Notably, the red fluorescence signals could be significantly diminished by LP-9220556 (a potent and selective hNotum inhibitor), confirming that the formation of fluorescent product from **IR-783 octanoate** was primarily mediated by hNotum in these cancer cells. Meanwhile, it was also noteworthy that the differences in fluorescence intensities of **IR-783 octanoate** stained cell lines were highly consistent with the hNotum expression levels (Fig. S6 in Supporting information), which were reported in our previous studies [28,29].

Interestingly, some extremely bright cells were observed in **IR-783 octanoate** stained SW620 cells (Fig. 4a). The brightly fluorescent signals generated in these cells suggested significantly elevated hNotum activity, which would infer the aberrant Wnt signaling pathway in these cells [1–3,5]. Hoechst staining of these cells showed unique feature of multipolar spindles [53–55], while the presence of multipolar spindles is often associated with supernumerary centrosomes (*i.e.*, centrosome amplification (CA)) and chromosomal instability [54,56]. Increasing studies have confirmed that CA is an early event widely present in precancerous lesions of cancers [54,57], which is closely related to Wnt signaling pathway. Considering that the aberrant Wnt signaling pathway may cause CA [57–60], the occurrence of multipolar spindles in these cells was probably associated with the CA triggered by the

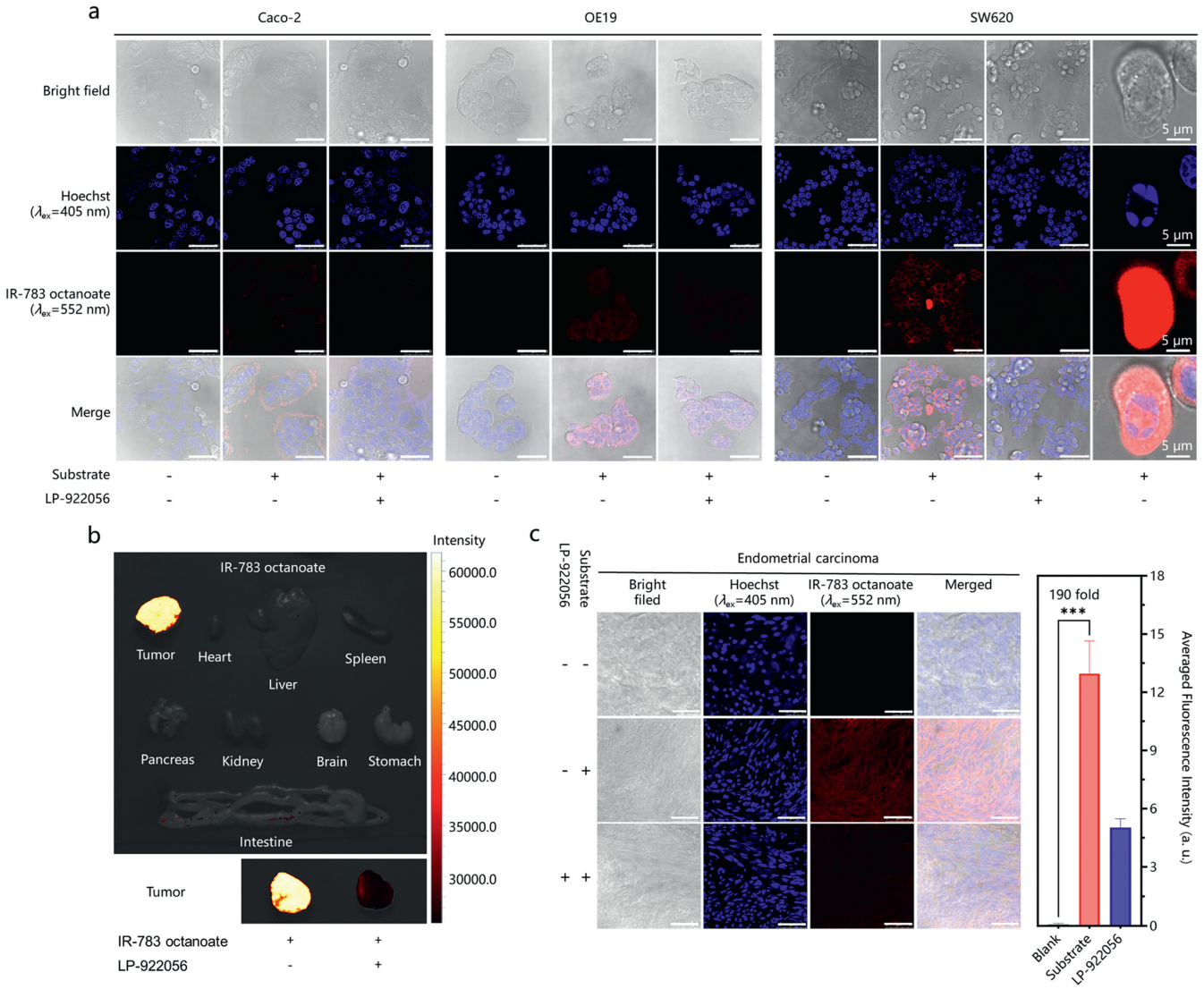

Fig. 4. (a) Functional imaging of hNotum in SW620, OE19 and Caco-2 cells using IR-783 octanoate. (b) Functional imaging of hNotum at the organelle level using IR-783 octanoate as a fluorogenic tool. (c) *In-situ* confocal imaging of hNotum functions in endometrial carcinoma samples. Quantification of averaged fluorescence intensities in the confocal imaging was done by the ROI tools of ImageJ, $^{***}P < 0.001$. Error bars represent mean ± standard error of mean (SEM). Unless marked separately, scale bar = 50 μm.

aberrant Wnt signaling. These observations suggested that **IR-783 octanoate** could be used as practical fluorogenic tool for visualizing the cells undergoing abnormal cell mitoses or accompanying with dysregulated Wnt signaling pathway, at the single-cell level.

Next, the transmembrane transport mechanism of **IR-783 octanoate** was investigated. Under physiological conditions, **IR-783 octanoate** is a charged molecule with a large molecular weight, it may hardly to penetrate the cell membrane simply by diffusion. Previous studies have reported that various Cy7 dyes are transported into living cells mainly *via* organic anion transporting polypeptides (OATPs), which are widely distributed in tumor cells and regulated by the cancer-related hypoxic-inducing factor-1α (HIF-1α) [61–63]. To confirm the transmembrane transport mechanism of **IR-783 octanoate**, sulfobromophthalein sodium (BSP, a specific OATPs inhibitor) was used in living SW620 cells. As shown in Fig. S7 (Supporting information), the fluorescence intensities inside from the cells could be significantly reduced upon addition of BSP, confirming that **IR-783 octanoate** was a good substrate for OATPs and the uptake of this agent into cells was mainly mediated by OATPs. Considering that OATPs is over-expressed in a variety of tumor cells and some solid tumors, which may strongly facilitate the uptake of **IR-783 octanoate** into cancerous cells and solid tumors.

To further investigate the uptake and imaging performance of **IR-783 octanoate** in solid tumors, SW620 cells-derived xenografts (CDX) model was established in mice and then imaged using **IR-783 octanoate** at the organelle level. As shown in Fig. 4b and Fig. S8 (Supporting information), brightly fluorescent signals were observed exclusively in the SW620-derived tumor, persisting for 72 h, while the signals could be significantly attenuated by LP-922056. These observations suggested that **IR-783 octanoate** showed favorable tumor permeability, outstanding photophysical properties and excellent selectivity towards hNotum at the organelle level, which encouraged us to perform *in-situ* functional imaging of hNotum in human cancerous tissues by using this novel imaging tool.

Finally, the hNotum activity in human endometrial carcinoma tissues are visualized using **IR-783 octanoate** as a fluorogenic tool. Previously studies have reported aberrant Wnt signaling in endometrial carcinoma [64–66], while genomics data also suggest high expression levels of hNotum in endometrial carcinoma [67–69]. As shown in Fig. 4c, upon addition of **IR-783 octanoate** in human endometrial carcinoma tissue slices for 30 min, brightly red fluorescence signals were observed, with an average enhancement of 190-fold. Upon addition of LP-922056, the red fluorescence signals were significantly decreased, suggesting that the red fluorescence signals were triggered mainly by hNotum in these cancerous tissues. These observations suggested that **IR-783 octanoate** could serve as a practical fluorogenic tool for hNotum-associated clinical carcinoma diagnosis and pathological investigations.

In summary, a suite of "T-shaped" Cy7 esters were rationally designed and synthesized aiming to get a novel and highly specific fluorogenic substrate for hNotum, on the basis of hNotum structure and its substrate preference. Following docking-based screening and experimental validation, **IR-783 octanoate** was validated as a novel enzyme-activatable fluorogenic tool, owing to this agent showed high affinity (0.98 ± 0.10 μmol/L) and excellent specificity towards hNotum. Under physiological conditions, **IR-783 octanoate** could be readily hydrolyzed to release a fluorogenic product (**IR-783 ketone**), which emitted long-wavelength emission around 646 nm. **IR-783 octanoate** was successfully used for *in-situ* functional imaging of hNotum in living cells and tumors, with high resolution and good tumor permeability. With the help of this novel fluorogenic tool, the functional heterogeneity of hNotum in different tumor cells were observed at the subcellular level, while a very high hNotum activity level was captured in SW620 cells with multipolar spindles. Collectively, this study devised a practical and highly specific visualization tool for *in-situ* functional imaging of hNotum in living systems, which would greatly facilitate *in-situ* monitoring the changes in hNotum activity under various conditions or tracking hNotum-related cellular events at the single-cell level.

Ethical statement

BALB/c (female, 6-weeks old) nude mice were acquired from the Shanghai University of Traditional Chinese Medicine and approved for use in the study by Shanghai University of Traditional Chinese Medicine Animal Care and Ethics Committee (Approval No. PZSHUTCM2304250007). All animal housing and experiments were conducted in strict accordance with the institutional guidelines for care and use of laboratory animals. Human cancer specimens from endometrial carcinoma were acquired from Liaoning Cancer Hospital & Institute, relative experimental procedures have been approved by the Ethics Committee of Liaoning Cancer Hospital & Institute (Ethical Approval No. 20220244), the study was performed in accordance with the 1964 declaration of HELSINKI and later amendments, written informed consent was obtained from all the participants prior to the enrollment of this study.

Declaration of competing interest

The authors declare that they have no known competing financial interests or personal relationships that could have appeared to influence the work reported in this paper.

Acknowledgments

This study was supported by National Natural Science Foundation of China (Nos. 81922070, 81973286, 82273897, U23A20516, 81801818), Shanghai Municipal Health Commission's TCM research project (No. 2022CX005), Innovation Team and Talents Cultivation Program of National Administration of Traditional Chinese Medicine (No. ZYYCXTDD-202004), Three-year Action Plan for Shanghai TCM Development and Inheritance Program (No. ZY(2021-2023)-0401), Department of Science & Technology of Liaoning Province Grant (No. 2022JH2/20200056), and supported by the State Key Laboratory of Fine Chemicals, Dalian University of Technology (No. KF 2202).

Supplementary materials

Supplementary material associated with this article can be found, in the online version, at doi:10.1016/j.cclet.2024.109601.

References

[1] R. Nusse, Cell Res. 15 (2005) 28–32.
[2] V.I. Torres, J.A. Godoy, N.C. Inestrosa, Pharmacol. Ther. 198 (2019) 34–45.
[3] C. Niehrs, Nat. Rev. Mol. Cell Biol. 13 (2012) 767–779.
[4] E.D. Bayle, F. Svensson, B.N. Atkinson, et al., J. Med. Chem. 64 (2021) 4289–4311.
[5] Y.H. Tian, X. Wang, Z. Cramer, et al., Gut 72 (2023) 2294–2306.
[6] J. Yu, D.M. Virshup, Biochem. Soc. Trans. 50 (2022) 1797–1808.
[7] S. Kakugawa, P.F. Langton, M. Zebisch, et al., Nature 519 (2015) 187–192.
[8] B. Madan, Z.Y. Ke, Z.D. Lei, et al., Oncotarget 7 (2016) 12386–12392.
[9] Y.G. Zhao, J.S. Ren, J. Hillier, et al., J. Pineal Res. 68 (2020) e12630.
[10] Y.G. Zhao, J.S. Ren, J. Hillier, et al., Commun. Biol. 3 (2020) 555.
[11] Y.F. Yuan, S. Wang, H. Zhou, et al., Front. Pharmacol. 13 (2022) 994995.
[12] K.H. Nilsson, P. Henning, M.E. Shahawy, et al., Am. J. Physiol. Endocrinol. Metab. 320 (2021) E967–E975.
[13] S. Movérare-Skrtic, K.H. Nilsson, P. Henning, et al., FASEB J. 33 (2019) 11163–11179.
[14] R. Brommage, J. Liu, P. Vogel, et al., Bone Res. 7 (2019) 2.
[15] N. Pentinmikko, S. Iqbal, M. Mana, et al., Nature 571 (2019) 398–402.
[16] J.W. Larrick, A.R. Mendelsohn, Rejuvenation Res. 22 (2019) 342–347.
[17] D.J. Flanagan, N. Pentinmikko, K. Luopajärvi, et al., Nature 594 (2021) 430–435.

[18] P.P. Yang, C.S. Li, Q. zhou, et al., Int. J. Biochem. Cell Biol. 153 (2022) 106316.
[19] Y. Liu, H. Chen, L.S. Xiao, et al., Cell. Oncol. 47 (2024) 463–480.
[20] Y. Torisu, A. Watanabe, A. Nonaka, et al., Cancer Sci. 99 (2008) 1139–1146.
[21] H. Gong, Q. Niu, Y. Zhou, et al., Bioengineered 12 (2021) 5241–5252.
[22] J.H. Yoon, D. Kim, J. Kim, et al., Cancer Genom. Proteom. 15 (2018) 485–497.
[23] Y. Xu, X.F. Wang, Y.M. Chu, et al., Ann. Transl. Med. 10 (2022) 169.
[24] L. Novellasdemunt, P. Antas, V.S.W. Li, Am. J. Physiol. Cell Physiol. 309 (2015) C511–C521.
[25] Q. Jin, L.L. Song, L.L. Ding, et al., Trends Anal. Chem. 152 (2022) 116620.
[26] R.J. Brommage, X. Feng, S. Hong, et al., Patent WO2012071381 (2012).
[27] J.H. Shi, B. Zhao, L.L. Song, et al., Chin. Chem. Lett. 35 (2023) 108405.
[28] L.L. Song, M.R. Sun, J.H. Shi, et al., Anal. Chem. 95 (2023) 5489–5493.
[29] M.R. Sun, L.L. Song, H.Z. Wei, et al., Sens. Actuators B: Chem. 393 (2023) 134145.
[30] P.X. Xiong, M.Y. Peng, J. Mater. Chem. C 7 (2019) 6301–6307.
[31] Y.G. Zhao, L. Schuhmacher, M. Roberts, et al., Mol. Metab. 49 (2021) 101201.
[32] L. Feng, W.J. Chen, X.X. Ma, et al., Org. Biomol. Chem. 18 (2020) 9385–9397.
[33] T.G. Liu, Y.L. Chen, H.Z. Wang, et al., Adv. Healthc. Mater. 12 (2023) e2202817.
[34] J.X. Wu, Z.X. Shi, L.L. Zhu, et al., Adv. Optical Mater. 10 (2022) 2102514.
[35] Y.S. Chen, L. Li, W.J. Chen, et al., Chin. Chem. Lett. 30 (2019) 1353–1360.
[36] L. Li, Y.S. Chen, W.J. Chen, et al., Chin. Chem. Lett. 30 (2019) 1689–1703.
[37] Z. Chang, F. Liu, L. Wang, et al., Chin. Chem. Lett. 30 (2019) 1856–1882.
[38] L. Strekowski, J.C. Mason, H. Lee, et al., J. Heterocycl. Chem. 41 (2004) 227–232.
[39] S. Genheden, U. Ryde, Expert Opin. Drug Dis. 10 (2015) 449–461.
[40] C. Hu, W. Sun, J.F. Cao, et al., Org. Lett. 15 (2013) 4022–4025.
[41] W.Q. Meng, Y.C. Chen, Y.W. Feng, et al., Org. Biomol. Chem. 16 (2018) 6350–6357.
[42] J.W. Ning, B.Z. Huang, Z.L. Wei, et al., Mol. Med. Rep. 15 (2017) 3761–3766.
[43] Y.Q. Song, G. Chen, X.Y. Han, et al., Sens. Actuators B: Chem. 286 (2019) 69–76.
[44] J.P. Wang, Y. Wen, F.J. Huo, C. Yin, Sens. Actuators B: Chem. 297 (2019) 126773.
[45] Y.C. Jiang, D. Jin, Y. Li, et al., Res. Chem. Intermed. 43 (2017) 2945–2957.
[46] K. Yin, F.B. Yu, W.W. Zhang, L.X. Chen, Biosens. Bioelectron. 74 (2015) 156–164.
[47] F.B. Yu, M. Gao, M. Li, L.X. Chen, Biomaterials 63 (2015) 93–101.
[48] S. Biswas, K. Kinbara, T. Niwa, et al., Nat. Chem. 5 (2013) 613–620.
[49] X. Wang, J. Sun, W.H. Zhang, et al., Chem. Sci. 4 (2013) 2551–2556.
[50] Z.Q. Guo, S. Nam, S. Park, J. Yoon, Chem. Sci. 3 (2012) 2760–2765.
[51] Y. Kim, Y. Choi, R. Weissleder, C.H. Tung, Biorg. Med. Chem. Lett. 17 (2007) 5054–5057.
[52] S. Tanaka, M. Hosokawa, T. Yonezawa, et al., Biol. Pharm. Bull. 38 (2015) 435–440.
[53] L.C. Cheng, J.C. Li, H.B. Sun, H.Y. Jiang, Phys. Rev. X 13 (2023) 011036.
[54] K. Mittal, J. Kaur, M. Jaczko, et al., Cancer Metastasis Rev. 40 (2021) 319–339.
[55] Y.X. Liang, W. Zhang, D.D. Li, et al., World J. Gastroenterol. 10 (2004) 2632–2636.
[56] H. Maiato, E. Logarinho, Nat. Cell Biol. 16 (2014) 386–394.
[57] M.M. Mahathre, P.C. Rida, R. Aneja, J. Biomed. Res. 30 (2016) 441–451.
[58] S. Bahmanyar, E.L. Guiney, E.M. Hatch, et al., J. Cell Sci. 123 (2010) 3125–3135.
[59] Q.J. He, P. Wang, Q.Q. Liu, et al., Am. J. Physiol. Cell Physiol. 318 (2020) C48–C62.
[60] K. Ruan, F. Ye, C.Y. Li, et al., PLoS One 7 (2012) e49184.
[61] M. Roth, A. Obaidat, B. Hagenbuch, Br. J. Pharmacol. 165 (2012) 1260–1287.
[62] C.H. Shi, J.B. Wu, G.C.Y. Chu, et al., Oncotarget 5 (2014) 10114–10126.
[63] X.J. Yang, C.M. Shi, R. Tong, et al., Clin. Cancer Res. 16 (2010) 2833–2844.
[64] I. Fatima, S. Barman, R. Rai, et al., Cancers 13 (2021) 2351.
[65] T.D. Bui, L. Zhang, M.C. Rees, et al., Br. J. Cancer 75 (1997) 1131–1136.
[66] Y.C. Dou, E.A. Kawaler, D.C. Zhou, et al., Cell 180 (2020) 729–748 e726.
[67] The Human Protein Atlas, 2020, https://www.proteinatlas.org.
[68] Gene Expression Profiling Interactive Analysis, 2020, http://gepia.cancer-pku.cn/index.html.
[69] The Cancer Genome Atlas Program, 2020, https://portal.gdc.cancer.gov/.